

A Data-driven Approach for Human Pose Tracking Based on Spatio-temporal Pictorial Structure

Soumitra Samanta and Bhabatosh Chanda

Abstract

In this paper, we present a data-driven approach for human pose tracking in video data. We formulate the human pose tracking problem as a discrete optimization problem based on spatio-temporal pictorial structure model and solve this problem in a greedy framework very efficiently. We propose the model to track the human pose by combining the human pose estimation from single image and traditional object tracking in a video. Our pose tracking objective function consists of the following terms: likeliness of appearance of a part within a frame, temporal displacement of the part from previous frame to the current frame, and the spatial dependency of a part with its parent in the graph structure. Experimental evaluation on benchmark datasets (VideoPose2, Poses in the Wild and Outdoor Pose) as well as on our newly build ICDPose dataset shows the usefulness of our proposed method.

I. INTRODUCTION

Human pose tracking is an important problem in computer vision due to its application in human action recognition and surveillance from video data. Visual appearance of any human action is a sequence of various human poses. We propose that if we can track those poses, then human action could be determined accurately. Human body is a symmetric articulated structure consisting of several parts connected pairwise. We define human pose as a combination of n parts (n depends on visible portion of a body). Let p_i denotes the i -th body part and $\mathbf{x}_i^t = (u_i^t, v_i^t)$ ($i = 1 : n$) its position in t^{th} frame. Where (u, v) is the image co-ordinate. Our aim is to track human pose in a video, i.e., to estimate the positions of these parts in every frame of the video. We write this as an optimization problem given by

$$\mathbf{x}_1^{t*}, \dots, \mathbf{x}_n^{t*} = \arg \min_{\mathbf{x}_1^t, \dots, \mathbf{x}_n^t} f(\mathbf{x}_1^t, \dots, \mathbf{x}_n^t | \mathbf{x}_1^{t-1}, \dots, \mathbf{x}_n^{t-1}) \quad (1)$$

In general, due to exponential search space of all body parts in all frames in a video, solving Eq. (1) is NP-hard. Researchers impose various constraints to limit the search space. Another major challenge in detecting these parts and subsequently the pose structure is *double counting*, which occurs due to symmetry in human body. In fact, the problem of double counting is resulted when detection score for each of the pair of symmetric parts becomes high at the same location because of occlusion. If not solved, this problem may affect subsequent processing such as pose estimation [31] and action recognition [3], [52], [22].

In this paper we model the human pose as a tree structure and develop a pose tracking algorithm where position of each body part is estimated based on its appearance in the current frame, position of its ancestor in the current frame, and its own position in the previous frame. Note that our model is different from the tree structure model proposed in [51]. We also propose a novel local part descriptor as the appearance of body part. Thus, our pose tracking algorithm is the combination of traditional object tracking [11] and pose estimation in still image [15]. Our main contributions in this paper are as follows.

- We propose a new human part descriptor based on sum of intensities and gradients over annular region that is computed efficiently using integral image.
- We propose a new objective function for human pose tracking in video data.
- In addition, we introduce a new full body human pose tracking dataset called ICDPose, which is more challenging and bigger than many state-of-the-art datasets. The dataset is available at [38] for research purpose.

Rest of the paper is organized as follows. Related works are briefly described in Section II. We present our proposed method in Section III which includes human part description, and model formulation for pose tracking. We evaluate the performance of our pose tracking method in Section IV which includes description of benchmark dataset, experimental setup, and comparison with the state-of-the-art methods. Finally, Section V concludes the paper.

II. RELATED WORKS

Equation (1) suggests that the position of a part in the current frame depends on its own position in the previous frame. This constraint helps in reducing the search space. If information from previous frame is not utilized, resultant algorithm can estimate human pose from a single image [51], [15], [27], [45], [34], [36], [24]. Almost all of these methods use pictorial structure model [17] explicitly for articulated human pose estimation, and differ primarily from one another in determining appearance and modeling the interaction among different parts in terms of constraints and a priori. For example, Yang et al. [51] capture

the local part as a mixture of different parts, while Dantone et al. [15] consider HOG features [14] and linear SVM as part appearance template. On the other hand, Kiefel and Gehler [24] model the presence and absence of body parts at every possible location of the image at any orientation and any scale. This results in a large number of binary random variables, which is handled more or less efficiently by approximate inference approach. Though many approaches employ efficient optimization solver for pose estimation (e.g., branch and bound based algorithm by Puwein et al. [34]), Ramakrishna et al. [36] have shown that modular framework along with symmetry property (left and right legs etc.) may lead to easy implementation and efficient inference without any efficient optimization solver. Dantone et al. [15] find the human pose using pairwise interdependencies of the parts and co-occurrence based joint regressors, while Ramakrishna et al. [36] exploit spatial interaction among multiple parts. Interdependencies of the parts are also handled by non-parametric Bayesian network [27]. In essence, all these methods adopt a common approach for human pose estimation, that is, by simultaneous identification of body parts (joints) as well as their interdependencies. On the other hand, Toshev et al. [45] adopted a holistic approach for human pose estimation using deep neural network. Deep convolutional neural network is also used for pose estimation [32] where temporal information from multiple frames is exploited. Human pose estimation from still image usually incur high computational cost (roughly 1 second for an image [51]). Second, these methods do not make use of temporal dependencies between locations of a part in subsequent frames. So, these methods are not directly employed to track human pose in video data.

In this paper our objective is to track the human pose in a video. To achieve this goal, our strategy is to track all the parts in the video subject to maintaining the tree structure representing the human body. Object tracking in a video has a rich repertoires of algorithms. Traditional object tracking [41], [60], [2], [20], [25], [56] [47], [8], [48], [58], [57], [29], [43], [55], [49], [50], [53], [44], [10], [12], [19], [54] algorithms generally search the target object in the current (t^{th}) frame within a search window around the target object location in the previous $(t - 1)^{th}$ frame. The target object is located by finding the maximum matching score between the target object template obtained from $(t - 1)^{th}$ frame and the patch at different locations within the search window in t^{th} frame. Variation in tracking strategy may lead to multiple object tracking [2] and nonrigid object tracking [25]. Zhang et al. [56] present a tracking method based on spatio-temporal context learning. They formulate the object tracking model as spatio-temporal relationships between the object of interest and its locally dense contexts in a Bayesian framework. They have used Fast Fourier Transform (FFT) to speedup the tracking process. Various other approaches such as Markov random field model [20] and sparse formulation [60], [5] are also adopted to track human figure.

Human pose tracking is significantly different from the traditional object tracking, as the former is a structurally combined representation of local parts. So, here the tracking method should not only track the local parts, but also have to maintain the global structure in terms of connectivity. Though an early work in this direction may be found in 1996 [23], because of complexity of the problem not many works on human pose tracking from video data has been reported so far. Some works consider restricted view of the human pose. For example, in [37] the authors assume that the people tend to take on a fixed set of canonical poses during activities and their algorithm can successfully detect the body parts in lateral walking pose. However, for the said task we may borrow the concept of still image pose estimation and incorporate inter-frame dependencies to perform tracking. Recently few researchers tried the same [35], [9]. Ramakrishna et al. [35] have modeled human body as a combination of singleton parts (e.g., head, neck) and symmetric pair of parts (e.g, left and right feet). So they formulate the pose tracking problem as a multi-target (parts) tracking problem where targets are related by an articulated structure. The appearance model and the optimization technique used to solve the problem incurs high computational cost. In [9] the authors propose a pose estimation model for video data by incorporating optical flow information in the pictorial structure model for still image [51]. As a result, computational complexity of the method becomes high. Some works on human pose tracking based on 3D data [16] [21], [4], [42], [40], [59], [7] are also available in the literature. We propose that we would estimate the human pose in the first frame of the video and then onward track the pose throughout the video. For the latter part of the task, we may employ object tracking algorithm to each part locally maintaining spatial relationship between pair of parts guided by a tree-structure.

III. PROPOSED METHOD

We simplify the problem stated in Eq. (1) with some rational assumptions and try to solve it within a reasonable time. We consider a human body pose in an image or frame as a graphical tree structure model, where each part or, more specifically ‘joint’ corresponds to a node of the graph and dependencies or physical link (based on human anatomy structure) between two parts define an edge of the graph (see brown colored structure in Fig. 1). In this model we consider head as the root of the tree structure, because among all the body parts head is unique and mostly visible, and can be detected with highest certainty [51].

Our main motivation of approximating the solution of (1) for human pose tracking is as follows. In human pose tracking, our ability to detect the position of each part in the current frame depends on the three factors: (i) the position of its ancestor in the current frame, (ii) its own position in the previous

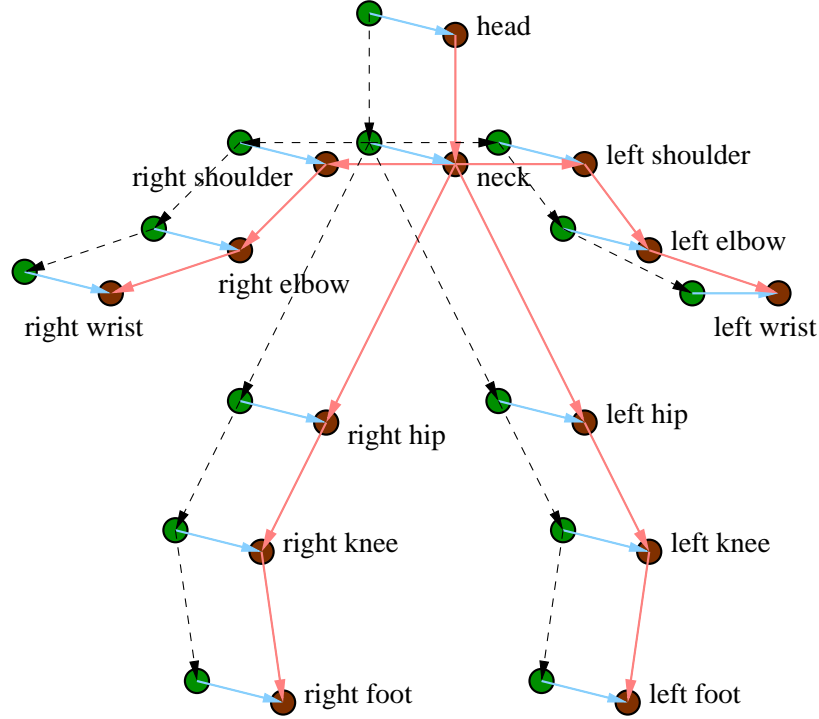


Fig. 1. Proposed human pose tracking structure. Brown colored nodes represent the tree structure in the t^{th} frame that we want to estimate, while the green colored nodes are the same in the $(t-1)^{th}$ frame, which are already known. The direct dependencies of a node are marked with arrow sign (\rightarrow).

frame, and (iii) its appearance in the current frame. In Fig. 1, brown colored nodes represent the tree structure in the t^{th} frame that we want to estimate, while the green colored nodes are the same in the $(t-1)^{th}$ frame, which are already known. The direct dependencies of a node are marked with arrow sign (\rightarrow). So, if we know the position of the root of the human body tree structure in the current frame and the nature of dependency of each node to its ancestors, then we can find the solution of (1) in polynomial time using greedy approach.

Given that position of a part p_i in $(t-1)^{th}$ frame is $\mathbf{x}_i^{(t-1)}$ and the position of its parent $p_{par(i)}$ in the t^{th} frame is $\mathbf{x}_{par(i)}^t$, we find the position \mathbf{x}_i^t of the part (node) p_i in the t^{th} frame as

$$\mathbf{x}_i^{t*} = \underset{\mathbf{x}_i^t}{arg \min} \{l_i(\mathbf{x}_i^t) + d_i(\mathbf{x}_i^{(t-1)}, \mathbf{x}_i^t) + d_{i,par(i)}(\mathbf{x}_i^t, \mathbf{x}_{par(i)}^t)\} \quad (2)$$

where $l_i(\mathbf{x}_i^t)$ measures the likeliness of appearance when the template of part p_i is placed at location \mathbf{x}_i^t in the t^{th} frame. Note that the image or feature representation of part p_i in $(t-1)^{th}$ frame is used as the template for that part in the t^{th} frame. The function $d_i(\mathbf{x}_i^{(t-1)}, \mathbf{x}_i^t)$ represents the amount of

temporal displacement of part p_i from $(t-1)^{th}$ frame to t^{th} frame. For a part p_i given its parent $p_{par(i)}$, $d_{i,par(i)}(\mathbf{x}_i^t, \mathbf{x}_{par(i)}^t)$ is a function which measures the deviation from expected spatial distance between part p_i and its parent in the t^{th} frame.

To find \mathbf{x}_i^{t*} we need to know $\mathbf{x}_{par(i)}^{t*}$ first. Similarly to know $\mathbf{x}_{par(i)}^{t*}$ we have to know $\mathbf{x}_{par(par(i))}^{t*}$ by solving the optimization problem (2) at appropriate level. In this way we recursively reach the root node of the pose tree structure. So we find the position of the root part p_{root} in t^{th} frame ignoring the term defining dependency to parent node in (2) as follows:

$$\mathbf{x}_{root}^{t*} = arg \min_{\mathbf{x}_{root}^t} \{l_{root}(\mathbf{x}_{root}^t) + d_{root}(\mathbf{x}_{root}^{(t-1)}, \mathbf{x}_{root}^t)\} \quad (3)$$

where the function $l_{root}(\mathbf{x}_{root}^t)$ measures the likeliness of appearance when the template of root part p_{root} is placed at location \mathbf{x}_{root}^t , and $d_{root}(\mathbf{x}_{root}^{(t-1)}, \mathbf{x}_{root}^t)$ measures the amount of temporal displacement as stated before.

We consider the objective functions (2) and (3) for pose tracking at possible position $\mathbf{x}_i^t \in W_i$, where W_i denotes a window around $\mathbf{x}_i^{(t-1)}$. The functions $d_i(\mathbf{x}_i^{(t-1)}, \mathbf{x}_i^t)$ and $d_{i,par(i)}(\mathbf{x}_i^t, \mathbf{x}_{par(i)}^t)$ actually play the role of constraints in estimating the part position \mathbf{x}_i^t , because in (2) $l_i(\mathbf{x}_i^t)$ measures the likeliness of appearance of part p_i between t^{th} and $(t-1)^{th}$ frames and we try to optimize it. Now depending on the speed of the movement and the rate of change in appearance of the part, reliability of each of the above terms varies. So we rewrite our objective function for each part p_i in a regularization form as,

$$\mathbf{x}_i^{t*} = arg \min_{\mathbf{x}_i^t} \{l_i(\mathbf{x}_i^t) + \lambda_1 d_i(\mathbf{x}_i^{(t-1)}, \mathbf{x}_i^t) + \lambda_2 d_{i,par(i)}(\mathbf{x}_i^t, \mathbf{x}_{par(i)}^t)\} \quad (4)$$

and

$$\mathbf{x}_{root}^{t*} = arg \min_{\mathbf{x}_{root}^t} \{l_i(\mathbf{x}_{root}^t) + \lambda_1 d_{root}(\mathbf{x}_{root}^{(t-1)}, \mathbf{x}_{root}^t)\} \quad (5)$$

where λ_1 and λ_2 are the regularization parameters controlling the importance of various terms in optimization.

To minimize the objective functions (4) and (5), we need to know the functions $l_i(\mathbf{x}_i^t)$, $d_i(\mathbf{x}_i^{(t-1)}, \mathbf{x}_i^t)$, for $i = 1 : n$ and $d_{i,par(i)}(\mathbf{x}_i^t, \mathbf{x}_{par(i)}^t)$ for $i = 2 : n$. We learn these functions from the training data and describe this learning process in the subsequent subsections.

A. Measure of likeliness of appearance

Measure of likeliness of appearance $l_i(\mathbf{x}_i^t)$ for each part p_i ($i = 1 : n$) in t^{th} frame is an important term for object detection and tracking. In human pose estimation this term is learned from the training data,

where HOG features are widely used [51]. In human pose tracking, use of fixed template may not work well because of movement, 3D to 2D projection and occlusion. So people try to match the raw pixel values of the part between $(t-1)^{th}$ and t^{th} frames using, say, sum of absolute differences (SAD) [33]. Here we measure the likeliness of appearance using Euclidean distance between feature vectors $\phi(\mathbf{x}_i^t)$ describing the appearance of the part p_i at location $\mathbf{x}_i^{(t)}$ in t^{th} frame and the corresponding template $\tau(\mathbf{x}_i^t)$ as

$$l_i(\mathbf{x}_i^t) = \|\phi(\mathbf{x}_i^t) - \tau(\mathbf{x}_i^t)\|_2 \quad (6)$$

Traditional methods form $\phi(\mathbf{x}_i^t)$ with raw pixel values and use $\tau(\mathbf{x}_i^{(t)}) = \phi(\mathbf{x}_i^{(t-1)})$. Here we describe each human part using a novel rectangular feature using *Integral image*. Thus the proposed feature can be computed more efficiently compared to state-of-the-art features (see computational complexity in Subsection IV-D). As our feature computation is based on Integral image representation, we briefly describe it next.

Integral image representation: Integral image was first appeared in graphics literature [13] and became popular in computer vision community after successful application in face detection [46]. Let I be an input image. Then integral image \bar{I} can be defined as

$$\bar{I}(x, y) = \sum_{1 \leq r \leq x; 1 \leq c \leq y} I(r, c) \quad (7)$$

i.e., $\bar{I}(x, y)$ stores the sum of all pixels above and left to the pixel (x, y) of input image I [Fig. 2(a)]. Integral image \bar{I} can be computed in a single pass over the input image I using the following recurrence relations.

$$S(x, y) = S(x, y-1) + I(x, y) \quad (8)$$

$$\bar{I}(x, y) = \bar{I}(x-1, y) + S(x, y) \quad (9)$$

where S is the cumulative row sum of image I with $S(x, 0) = 0$ and $\bar{I}(0, y) = 0$. The advantage of \bar{I} is that the sum of pixel values in any rectangular region ABCD [Fig. 2(b)] of I can be computed as $\bar{I}(D) + \bar{I}(A) - \bar{I}(B) - \bar{I}(C)$, i.e., using only three arithmetic operations, which is quite fast.

Proposed local feature computation: For human body part description the main challenge is the deformation in appearance as well as its rotation. For example, consider the *elbow* part in action where joint angle changes frequently (see Fig. 3), and due to that the traditional features (e.g, raw pixel values or different variants of gradient histogram based features) may not work well. So to represent a human body part we consider m concentric rectangular annular strip around the center of that part as shown in

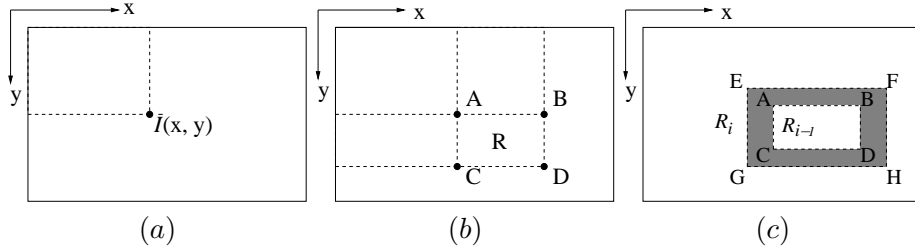


Fig. 2. Integral image representation and rectangular region feature calculation: (a) integral image, (b) sum of the pixels value within the region R can be computed using $[(A+D) - (B+C)]$, and (c) sum of pixel values within the region $R_i \setminus R_{i-1}$ (shaded region) can be computed using $[\{(E+H) - (F+G)\} - \{(A+D) - (B+C)\}]$.

Fig. 2(c) and mark them as R_1, \dots, R_m in ascending order of their areas. Now sum of pixel values within the annular region $a_i = R_i \setminus R_{i-1}$ ($i = 1 : m$, with $R_0 = \Phi$) can be computed very efficiently using integral image representation. We calculate the sum of pixel values within the region a_i by subtracting sum over R_{i-1} from the sum over R_i .

For each color channel we compute m sum values for intensity, magnitude of horizontal gradient and magnitude of vertical gradient separately. We normalize these sum values by their corresponding area. Thus we get $9m$ dimensional feature vector at each location of human body part.

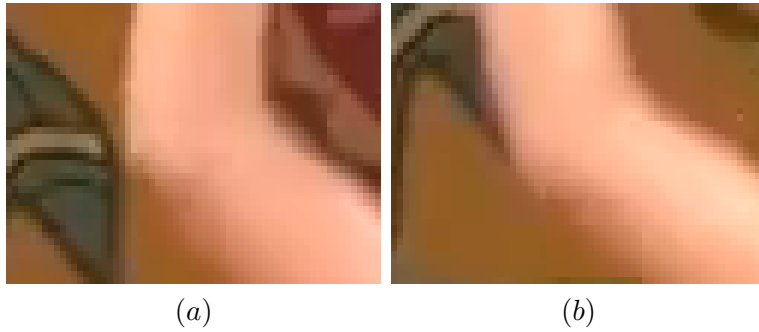


Fig. 3. Elbow part in two consecutive frames of ICDPose dataset.

Occlusion of parts causes a big problem in human pose tracking. To overcome this issue we update the body part template based on the previous frames. This learned template helps in describing the modified part more reliably under occlusion as well as deformation. After estimating x_i^t in t^{th} frame, we update the template $\tau(\mathbf{x}_i^{t+1})$ for p_i ($i = 1 : n$) in the $(t + 1)^{th}$ frame as

$$\tau(\mathbf{x}_i^{t+1}) = \alpha\phi(\mathbf{x}_i^t) + (1 - \alpha)\tau(\mathbf{x}_i^{(t)}) \quad (10)$$

where $\alpha = e^{-l_i(\mathbf{x}_i^t)}$. Note that the proposed feature vector as well as the template as rotation, translation

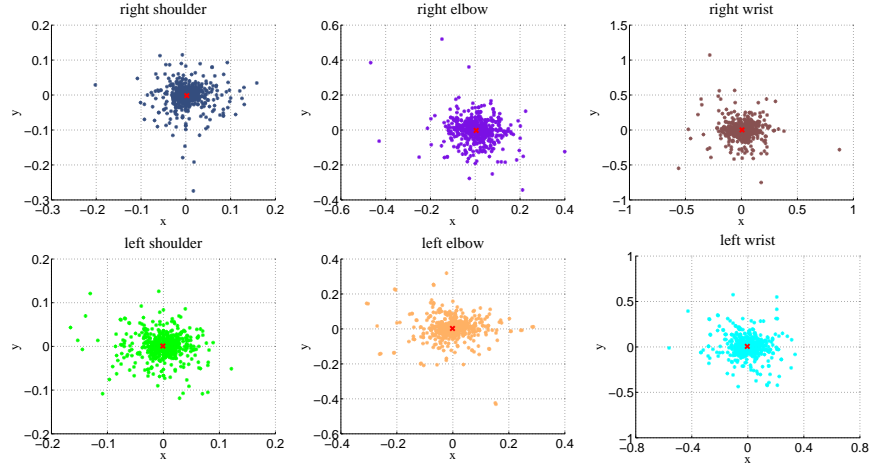


Fig. 4. Temporal displacement of different parts of VideoPose2 training database.

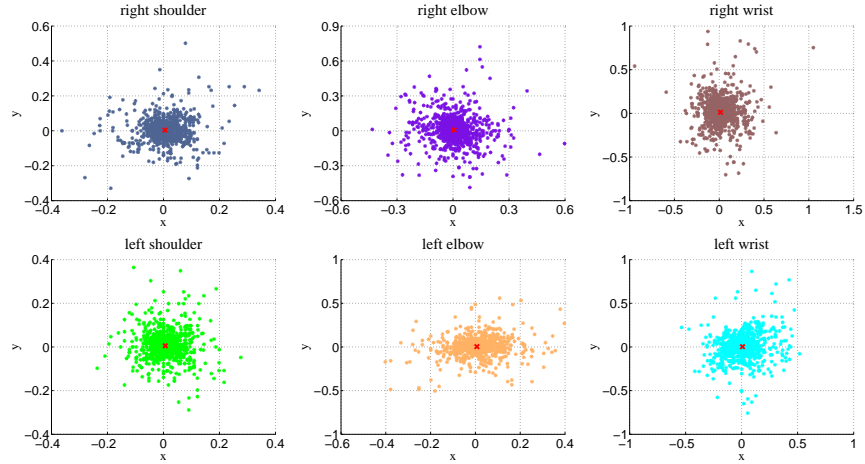


Fig. 5. Temporal displacement of different upper body parts of ICDPose training dataset.

and flip invariant.

B. Temporal displacement

We have defined the amount of temporal displacement $d_i(\mathbf{x}_i^{(t-1)}, \mathbf{x}_i^t)$ of each part p_i ($i = 1 : n$) in the data driven framework. From the training data we calculate temporal displacement $\mathbf{e}_i = \mathbf{x}_i^t - \mathbf{x}_i^{(t-1)}$ from $(t - 1)^{th}$ frame to t^{th} frame. Thus, for each part p_i we have a set of temporal displacement \mathbf{e}_i . Fig. 4 show the temporal displacement of different parts (left and right shoulders, left and right elbows, and left and right wrists) from VideoPose2 training dataset. Temporal displacement of ICDPose training data

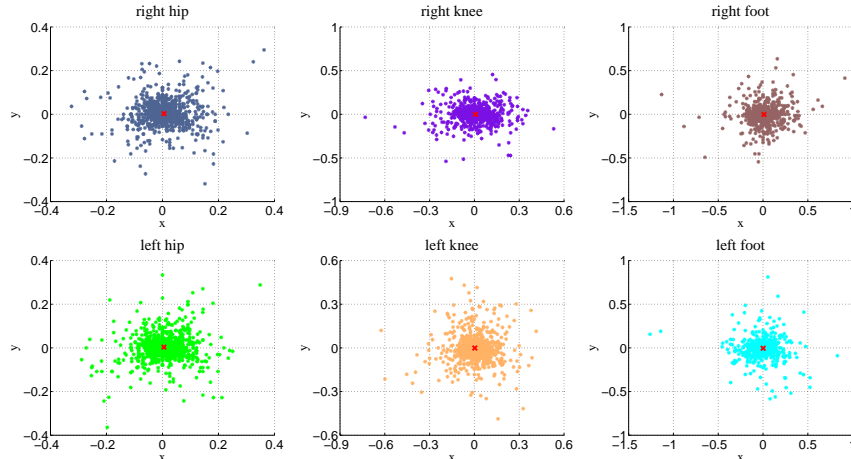


Fig. 6. Temporal displacement of different lower body parts of ICDPose training dataset.

for different parts are shown in Fig. 5 and 6. Observing these three figures we postulate that a bivariate Gaussian distribution may represent the temporal displacement of each part. So, from the set of \mathbf{e}_i 's, we learn a Gaussian distribution (μ_i, Σ_i) for each part p_i ($i = 1 : n$). We use Mahalanobis distance from the learned distribution for \mathbf{e}_i 's to define $d_i(\mathbf{x}_i^{(t-1)}, \mathbf{x}_i^t)$ of part p_i in t^{th} frame as,

$$d_i(\mathbf{x}_i^{(t-1)}, \mathbf{x}_i^t) = (\mathbf{e}_i - \mu_i)^T \Sigma_i^{-1} (\mathbf{e}_i - \mu_i) \quad (11)$$

where $\mathbf{e}_i = \mathbf{x}_i^t - \mathbf{x}_i^{(t-1)}$ is the temporal displacement of part p_i from $(t-1)^{\text{th}}$ frame to t^{th} frame.

C. Spatial deformation

Distance between two parts may change in 2D frame due to change in orientation of the portion of the body connecting two said parts in 3D. We call this change in distance as a result of 3D to 2D mapping as *spatial deformation*. This spatial deformation is handled through the dependency of a body part node of the pose tree structure on its parent part. In traditional pose estimation or object recognition model, researchers have captured this dependency by relative position of that part p_i with respect to its parent connected by an edge. In [17] the degree of deformation of a part with respect to the other is modeled by a Gaussian distribution of their relative position. We use similar idea with a little modification to model our part dependency relation in data driven framework. We compute the relative position of part p_i with respect to its parent $p_{\text{par}(i)}$ position from the training data. Fig. 7 and 8 shows the relative positions of each parts (left and right shoulder with respect to neck; left and right elbow to the left and right

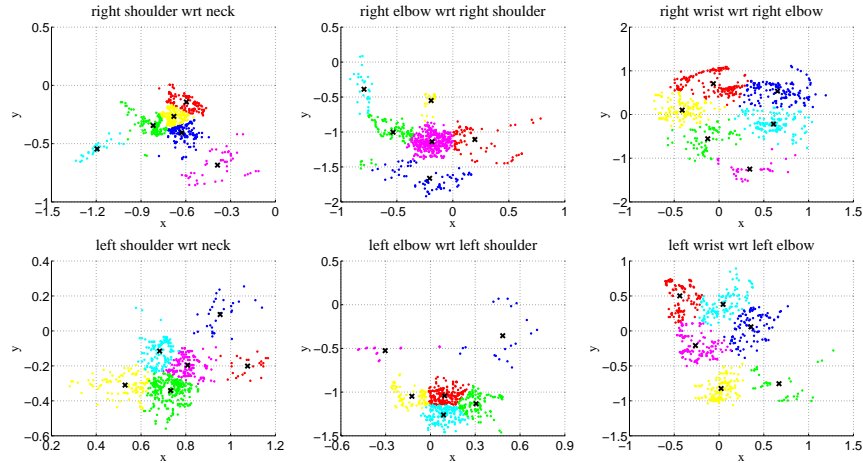


Fig. 7. Different body part positions with respect to (wrt) its parent position of Videopose2 training database.

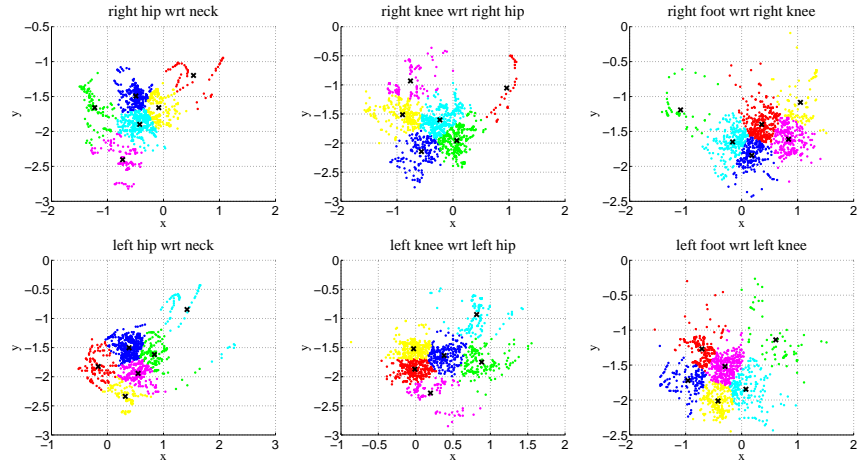


Fig. 8. Different upper body part positions with respect to (wrt) its parent position of ICDPose training database.

shoulder respectively; and left and right wrist to the left and right elbow respectively) for VideoPose2 and ICDPose dataset respectively. Fig. 9 shows the relative positions of lower body parts (left and right hips and relatively lower) of ICDPose dataset. From these three figures we observe that one Gaussian distribution for each part is not sufficient to capture its dependency relation. Instead we make the system learn multiple Gaussian distributions for each part to capture the part’s spatial dependency.

To learn multiple Gaussian distributions, we use the data driven approach [51]. We first cluster the relative positions of each part using k-means clustering algorithm. Figs. 7, 8, and 9 show the clusters of relative locations of different parts of VideoPose2 and ICDPose datasets. Then we learn a Gaussian

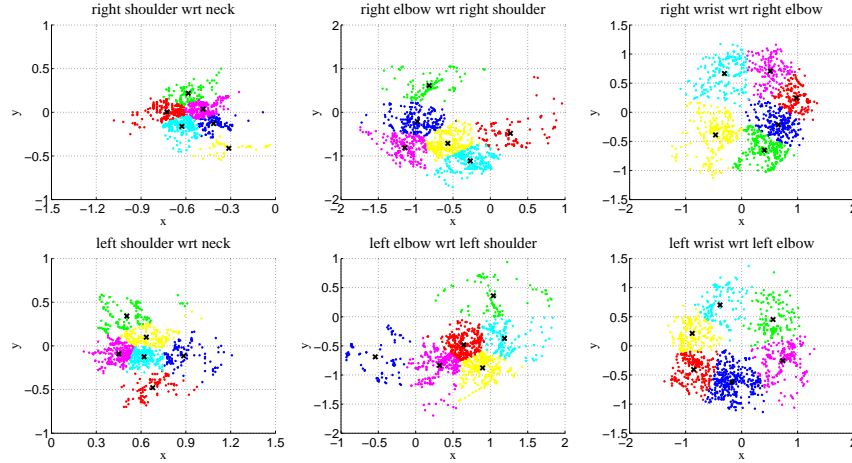


Fig. 9. Different lower body part position with respect to (wrt) its parent position of ICDPose training database.

distribution $(\mu_{i,par(i)}^c, \Sigma_{i,par(i)}^c; c = 1 : N_i)$ ($i = 2 : n$) for each cluster separately, where N_i is the number of clusters of relative position for part p_i . Similar to temporal displacement, here also we use Mahalanobis distance measure to define the degree of deformation $d_{i,par(i)}(\mathbf{x}_i^t, \mathbf{x}_{par(i)}^t)$ of a part p_i ($i = 2 : n$) with respect to its parent $p_{par(i)}$ as,

$$d_{i,par(i)}(\mathbf{x}_i^t, \mathbf{x}_{par(i)}^t) = \min_{\substack{\mu_{i,par(i)}^c, \Sigma_{i,par(i)}^c \\ c=1:N_i}} \{(\mathbf{e}_{i,par(i)} - \mu_{i,par(i)}^c)^T (\Sigma_{i,par(i)}^c)^{-1} (\mathbf{e}_{i,par(i)} - \mu_{i,par(i)}^c)\} \quad (12)$$

where $\mathbf{e}_{i,par(i)} = \mathbf{x}_i^t - \mathbf{x}_{par(i)}^t$ is the relative displacement of part p_i with respect to its parent $p_{par(i)}$.

D. Tracking human pose in a video

After getting all the parameters for the functions $l_i(\mathbf{x}_i^t)$, $d_i(\mathbf{x}_i^{(t-1)}, \mathbf{x}_i^t)$, ($i = 1 : n$) and $d_{i,par(i)}(\mathbf{x}_i^t, \mathbf{x}_{par(i)}^t)$ ($i = 2 : n$) we plugin the optimization problems (4) and (5) for the human pose tracking in a video. Now for tracking a human pose in a video, we need the human pose at the first frame of that video. We may manually annotate the human pose at the first frame or may employ a good human pose estimation algorithm for still image, and then track that pose through all the frames of that video using our proposed pose tracking model. Thus our human pose tracking method for a video clip works as follows: We manually annotate a human pose in the first frame of a video and our aim is to track that pose through all the frames of that video. As we have mentioned that human head is the root part of our pose structure. So, for the second frame we first track the head part using (5) and then track all the

remaining parts using (4) in a greedy fashion. In a similar way, given a human pose in the k^{th} frame we track the pose in the $(k + 1)^{th}$ frame of that video. Our algorithm first fixes the root node and travels from parent $p_{par(i)}$ position $\mathbf{x}_{par(i)}^{t*}$ of a part p_i to position \mathbf{x}_i^{t*} of part p_i . So, computational complexity to track each part is linear in the possible location of each part p_i with a constant multiplier (number of clusters of relative location of part p_i). Let for each part p_i ($i = 1 : n$) we have M possible locations and N number of clusters for each of these relative locations. Then the time complexity of our proposed method is $O(nMN)$ per frame. We evaluate our proposed human pose tracking method using standard benchmark datasets and compare with the state-of-the-art methods discuss in the next Section IV.

IV. EXPERIMENTAL RESULT

We have implemented our algorithm in MATLAB2013a and evaluated in a system with Intel(R) Core(TM) i5-2430M CPU @ 2.40 GHz and 4GB RAM running Windows 7 operating system. We evaluate our proposed method on benchmark datasets as well as on our new dataset. In this section we briefly describe each of the datasets followed by experimental settings.

A. Datasets

Here we have used three benchmark datasets: VideoPose2 [39], Poses in the Wild [9] and Outdoor Pose [35], and our new dataset ICDPose [38].

VideoPose2 dataset¹: This dataset is created from the TV shows *Friends* and *Lost*. The dataset contains 44 video clips with a total of 1286 frames. The dataset focuses on only the upper portion of body. Body parts such as torso, shoulders, elbows and wrists are manually annotated in all the frames. The authors have indicated the data partition for training (26 video clips) and test (14 video clips). We have followed this partition in our experiment.

Poses in the Wild dataset²: This dataset consists of 30 video clips with a total of 830 frames. The authors have created this dataset from Hollywood movies *Forrest Gump*, *The Terminal*, and *Cast Away*. This dataset too focuses on the upper portion of body with manually annotated parts: neck, shoulders, elbows, wrists and mid-torso.

ICDPose dataset³: Our Indian classical dance pose (ICDPose) dataset contains full body pose data. It has 60 video clips covering six most popular Indian classical dance styles (Bharatnatyam, Kathak,

¹<http://vision.grasp.upenn.edu/cgi-bin/index.php?n=VideoLearning.VideoPose2>

²<https://lear.inrialpes.fr/research/posesinthewild/>

³http://www.isical.ac.in/~vlrg/sites/default/files/Soumitra/Site/ss_icdpose.html

Kuchupudi, Mohiniyattam, Manipuri and Odissi). Each video clip has 45 frames with a total of 2700 frames in the whole dataset, which is sufficiently larger than the other benchmark datasets. This dataset is created from YouTube video library, where all the videos depict stage performance of Indian classical dancers. So our dataset has huge variations in respect of lighting condition, camera position, and clothing. We have manually annotated the following 14 body parts: head, neck, shoulders, elbows, wrists, hips, knees and feet. We have arbitrarily marked 5 video clips of each dance style as train data (30 video clips altogether) and the remaining 30 video clips as test data.

Outdoor Pose dataset⁴: This is a full body pose dataset. It consists of 6 videos where 4 different actors perform different actions in a outdoor environment. It has total 828 frames each with annotated 14 body joints (head, neck, shoulders, elbows, wrists, hips, knees and feet).

B. Experimental settings

Like all others, in our proposed human pose tracking algorithm some parameters need to be fixed. We choose these parameters experimentally based on training samples of VideoPose2 dataset and use most of these relevant parameter values for other datasets. For body part descriptor we fix $m = 10$ (see section IV-C) as the number of concentric annular regions for all the experiments. We have used maximum likelihood parameter estimation method to estimate the parameters of the Gaussian distribution for temporal displacement of each part. For each part different datasets exhibit different relative displacement distribution (see Fig. 7, 8 and 9). We have experimentally seen that for each part over all datasets six Gaussian distribution functions can represent the relative displacement faithfully. So we fix the number of clusters $k = 6$ and use maximum likelihood parameter estimation method to estimate the Gaussian distribution parameters of each cluster. Two regularization parameters are fixed as $\lambda_1 = 0.7$ and $\lambda_2 = 0.2$ experimentally based on VideoPose2 dataset.

Evaluation metric: We use the key point localization error as the evaluation metric [39]. In this metric, for each body part (joint), we calculate the pixel location deviation, i.e., the distance between the estimated location and corresponding ground truth location. Then for a video we compute the percentage of frames, where this distance is less than an acceptable deviation threshold Ω as average accuracy. Here we present the results for $\Omega = 5, 10, 15, 20, 25, 30, 35,$ and 40 pixels.

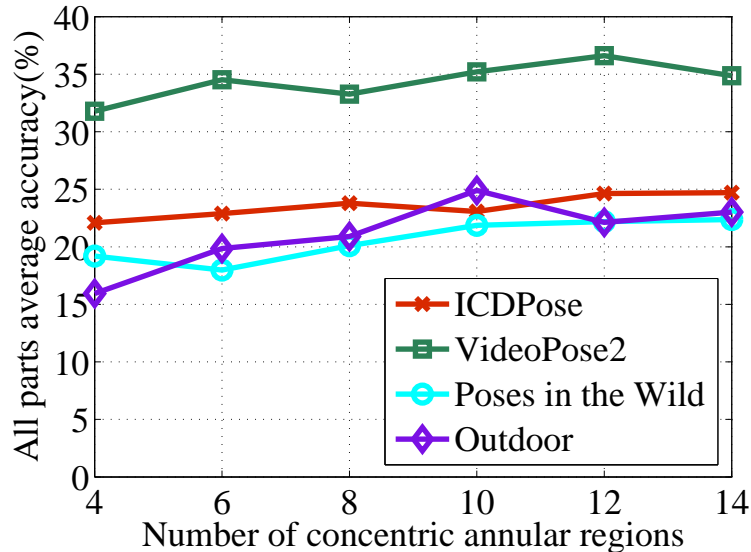


Fig. 10. Comparative results of tracking body parts using proposed descriptor with different number of concentric annular regions on different datasets (VideoPose2, Poses in the Wild, ICDPose and Outdoor Pose)

C. Experimental evaluation and discussion

Proposed feature evaluation: First, we determine the number m of concentric annular regions to describe body parts (joints) by proposed methods. We have tried different values of m from 4 to 14, and calculated the average accuracy of locating all body parts in various datasets ($\Omega = 5$). The results are summarised in Fig. 10. The experiment suggests $m = 10$ considering cost and accuracy. We then evaluate the performance of proposed part descriptor for conventional object tracking and compare it with other standard descriptors like RGB-histogram, HOG [14], RIFT [26], SIFT [28], and SURF [6] features. We track each part of the human body independently over a video based on their appearance measure only. Here similarity is measured using Euclidean distance between the descriptor template and the relevant frame. Figs. 11, 12, 13, and 14 show the average accuracy in tracking different body parts using various features for VideoPose2, Poses in the Wild, ICDPose and Outdoor Pose datasets respectively. From these figures we see that the proposed feature gives better or at least comparable result compared to the others. These figures also suggest that the accuracy decreases if we move from slow moving part to faster moving parts (i.e., shoulder to elbow to wrist).

Table I shows the average time taken to process each frame (in second) of various datasets and reveals

⁴<http://www.cs.cmu.edu/~vramakri/Data/>

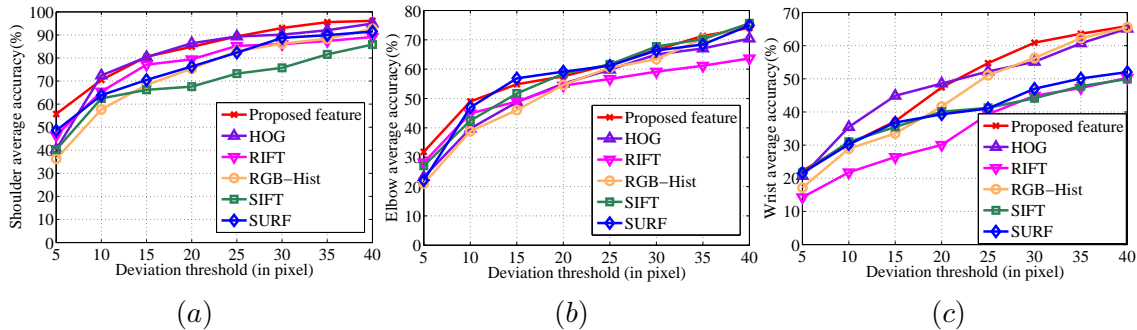


Fig. 11. Comparative results of tracking different body parts independently using different features on VideoPose2 dataset: (a) shoulder, (b) elbow, and (c) wrist.

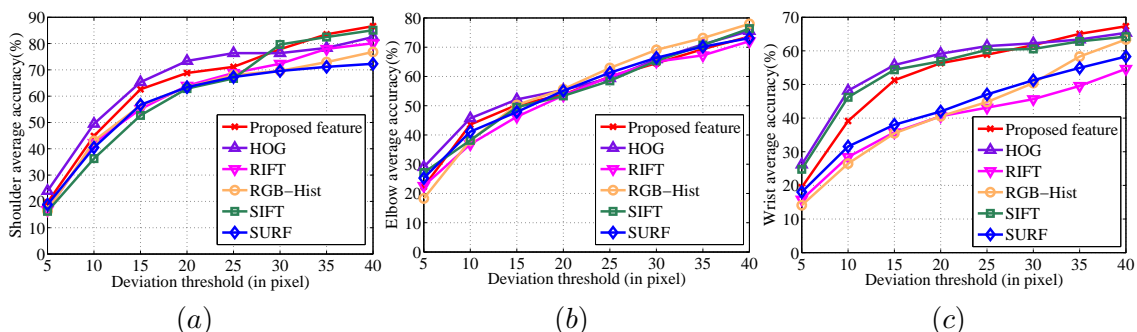


Fig. 12. Comparative results of tracking different body parts independently using different features on Poses in the Wild dataset: (a) shoulder, (b) elbow, and (c) wrist.

that the proposed feature computation is faster than the others. We have already mentioned that (in first paragraph of Section IV) our feature implementation has been done in MATLAB (with no mex file interface). For other feature like HOG, we have used Yang et al. [51] implementation with bin size 4. We have implemented the RIFT feature in MATLAB with parameters suggested in [26] (i.e., four concentric ring and eight histogram orientation). For SURF feature, we have used MATLAB R2013a SURF feature implementation. We have used Ce Liu’s dense SIFT feature implementation with default parameters [1].

So based on the experimental observations stated in the previous paragraph we use the proposed descriptor to track the human pose in all the datasets by optimizing the objective functions (4) and (5). We compare our result for human pose tracking with that of the state-of-the-art pose estimation methods [39], [30] and [9]. We also compare our results with that of the state-of-the-art individual object tracking methods [41], [56], where each of the body parts separately fed to these methods and each body part is treated as a single object. These two methods are brought into comparison to show the effect of spatial

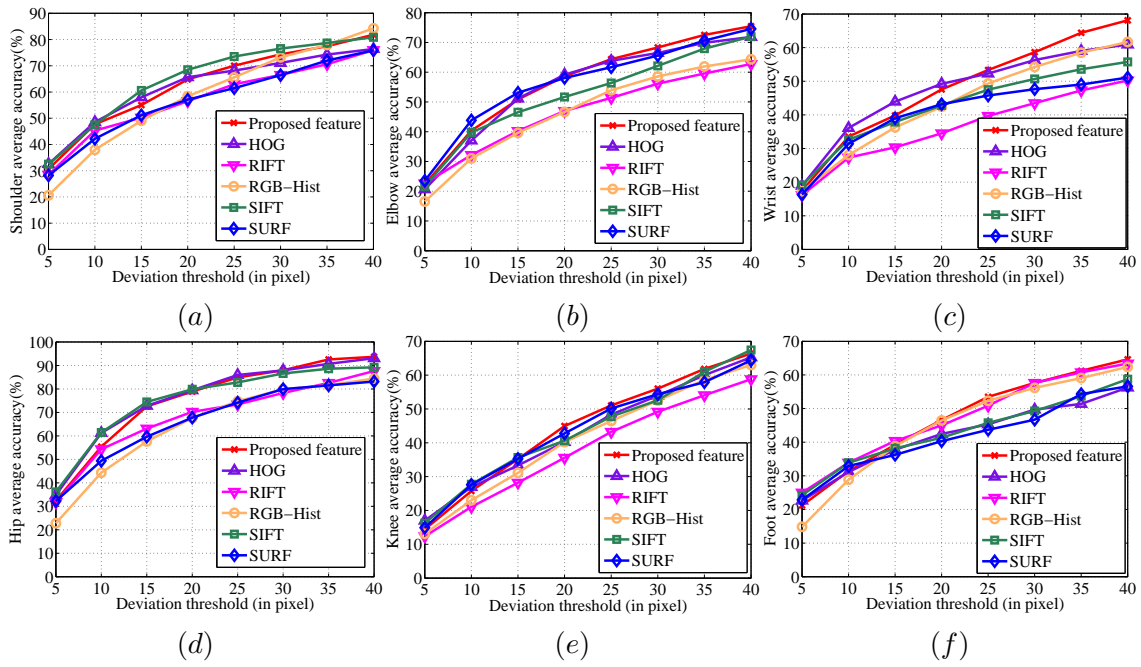


Fig. 13. Comparative results of tracking different body parts independently using different features on ICDPose dataset: (a) shoulder, (b) elbow, (c) wrist, (d) hip, (e) knee, and (f) foot.

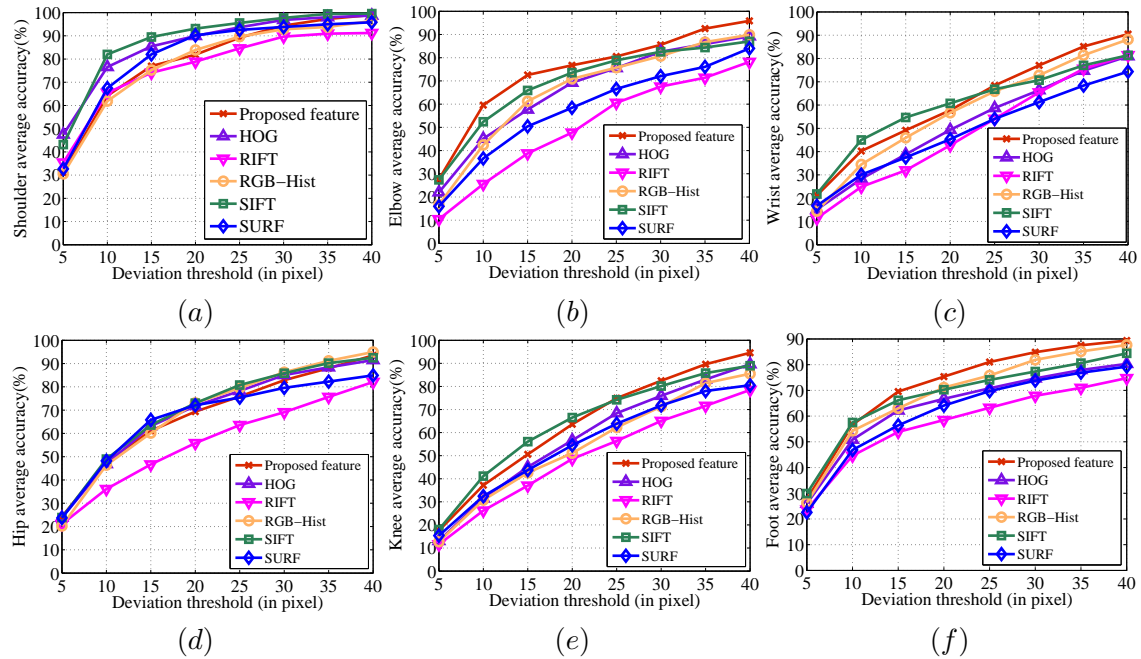


Fig. 14. Comparative results of tracking different body parts independently using different features on Outdoor Pose dataset: (a) shoulder, (b) elbow, (c) wrist, (d) hip, (e) knee, and (f) foot.

TABLE I
AVERAGE TIME COMPARISON (IN SEC./FRAME) OF PROPOSED FEATURE WITH OTHERS ON DIFFERENT DATASETS.

Datasets	RGB-hist	HOG [14]	RIFT [26]	SIFT [28]	SURF [6]	Proposed
VideoPose2 [39]	1.0173	1.1166	1.1147	0.2277	1.5360	0.1901
Poses in the Wild [9]	1.0527	1.1011	1.1848	0.2365	1.5469	0.1993
ICDPose [38]	1.8711	1.6978	1.8157	0.5040	2.7237	0.4396
Outdoor Pose [35]	1.7909	1.6121	1.7402	0.4144	2.5802	0.3527

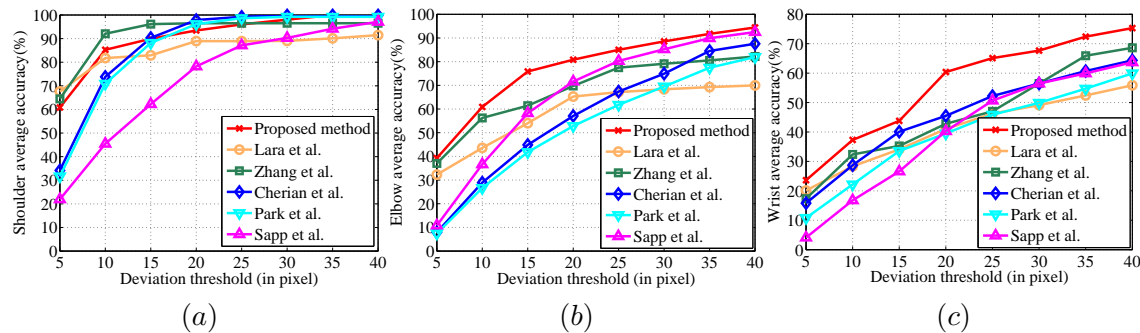


Fig. 15. Comparative results of proposed method with the state-of-the-art methods for human pose tracking on VideoPose2 dataset: (a) shoulder, (b) elbow, and (c) wrist.

constraints provided by the connected body parts over the independent individual part tracking. Note that for all these methods we have used their implementation with default parameter settings.

Experimental results on VideoPose2 dataset: For VideoPose2 dataset we use the authors suggested training and test data partition. Fig. 15 shows the comparison for different body parts like shoulder, elbow, and wrist with the state-of-the-art methods. We see that in most of the cases our method gives the superior results. Note that since motion is less in the videos of this dataset, individual part tracking methods [41], [56] perform better than pose tracking methods [39], [30], [9]. However, the latter overtakes the formers when motion is more, i.e., for higher value of threshold. Aggregated results for all the parts and all the methods are shown in Table II.

Experimental results on Poses in the Wild dataset: Poses in the Wild dataset has no training and test data partition. We use first 15 video clips to train our system and the remaining 15 video clips to test. Note that we have followed the same data partition for all the methods. Fig. 16 shows the result of different methods on three individual body parts for comparison, and Table III shows average accuracy (%) for all three parts. Fig. 16(a) shows that our method gives better result for almost all the values of deviation threshold as the movement of this part is small. As the movement increases, performance of

TABLE II
AVERAGE ACCURACY (IN %) OF POSE TRACKING COMPRISING THREE PARTS (SHOULDER, ELBOW, AND WRIST) TOGETHER USING DIFFERENT METHODS ON VIDEOPOSE2 DATASET.

Dev. thrs. (in pixel)	Different methods					
	Lara [41]	Zhang [56]	Sapp [39]	Park [30]	Cherian [9]	Proposed
5	39.99	39.61	12.28	16.62	19.29	41.22
10	51.21	60.20	32.94	39.88	43.80	61.13
15	57.00	64.26	49.02	54.48	58.40	69.84
20	65.08	69.66	63.36	62.81	66.79	78.21
25	67.44	73.66	72.70	68.74	72.94	82.02
30	68.81	77.35	77.32	72.87	77.05	84.73
35	70.58	80.97	81.33	77.12	81.67	88.04
40	72.42	82.42	84.42	80.35	83.91	89.90

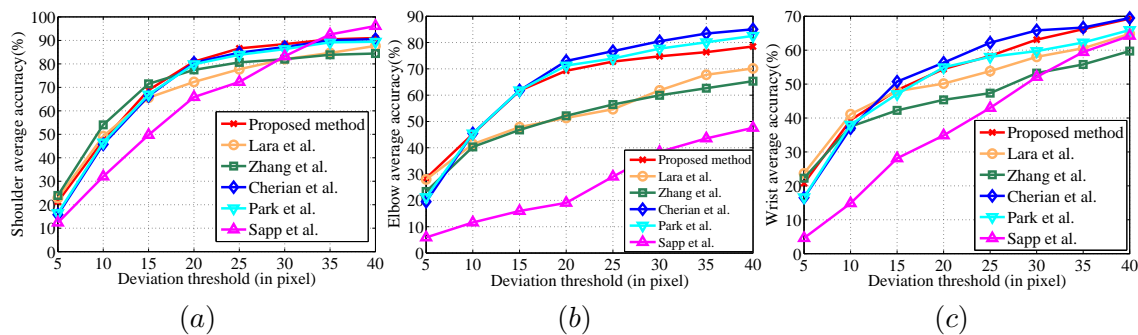


Fig. 16. Comparison results of different parts with the state-of-the-art methods on Poses in The Wild dataset: (a) shoulder, (b) elbow, and (c) wrist.

proposed method reduces, but it still remains within top two methods and far better than the individual object tracking methods [41], [56] as shown in Fig. 16(b) and (c) and Table III. Note that time complexity of the closest competitors [30], [9] is much higher than the proposed method (see Subsection IV-D).

Experimental results on ICDPose dataset: We have tested the proposed method on 30 video clips of ICDPose dataset using remaining 30 video clips as training data. Comparison of our results with the state-of-the-art methods are reported in Fig. 17 for different body parts. Figs. 17(e) and (f) show that the proposed method achieves highest scores for knee and foot, and for other parts it consistently remains among the top performers. However, for wrist part the proposed method falls marginally behind most of other methods as seen in Fig. 17(c). If we consider average accuracy computed over all body parts, the proposed method stands superior. However, for only upper portion of the body it stands third position (shown in Table VII).

Experimental results on Outdoor Pose dataset: Outdoor Pose dataset has also no training and test

TABLE III
AVERAGE ACCURACY (IN %) OF POSE TRACKING COMPRISING THREE PARTS (SHOULDER, ELBOW, AND WRIST) TOGETHER USING DIFFERENT METHODS ON POSES IN THE WILD DATASET.

Dev. thrs. (in pixel)	Different methods					
	Lara [41]	Zhang [56]	Sapp [39]	Park [30]	Cherian [9]	Proposed
5	24.82	23.19	7.63	18.08	17.27	23.50
10	43.91	43.94	19.48	43.32	42.72	44.02
15	53.78	53.51	31.27	58.60	59.59	59.57
20	57.93	58.31	39.93	68.67	69.93	68.21
25	62.04	61.47	48.11	71.94	74.56	72.55
30	67.28	65.06	57.93	74.56	77.82	75.42
35	70.99	67.43	65.17	77.19	80.03	77.67
40	74.19	69.82	69.31	79.29	81.67	79.59

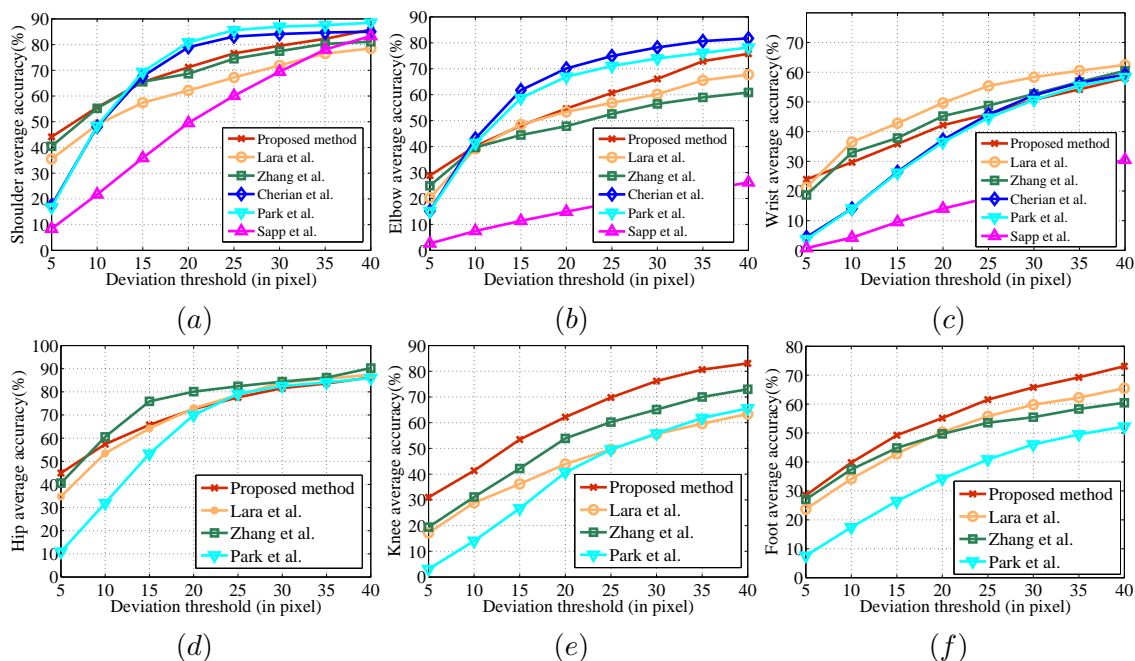


Fig. 17. Comparison results of different body parts with the state-of-the-art methods on ICDPose dataset: (a) shoulder, (b) elbow, (c) wrist, (d) hip, (e) knee, and (f) foot.

data partition. As it is a full body pose dataset, we obtain parameter values from ICDPose training dataset and use all the six videos as test data. This dataset has on average 138 frames per videos, which is large compared to other datasets like VideoPose2, Poses in the Wild and ICDPose. So we initialize our tracking method after every 60 frames. Fig. 18 shows the results of different body parts (joints) tracking using different methods for comparison. From this figure we see that performance of the proposed method is at least second best for individual parts, and is best considering average accuracy over all the parts as

TABLE IV
AVERAGE ACCURACY (IN %) OF POSE TRACKING COMPRISING UPPER BODY PARTS (WITHOUT BRACKET) AND FULL BODY PARTS (WITHIN THE BRACKET) TOGETHER USING DIFFERENT METHODS ON ICDPOSE DATASET.

Dev. thrs. (in pixel)	Different methods					
	Lara [41]	Zhang [56]	Sapp [39]	Park [30]	Cherian [9]	Proposed
5	25.67 (25.44)	28.01 (28.50)	03.93	11.89 (09.54)	12.35	32.28 (33.53)
10	41.50 (40.16)	42.61 (42.81)	11.16	34.62 (27.88)	35.07	41.79 (43.98)
15	49.56 (48.64)	49.29 (51.80)	18.95	51.42 (43.44)	51.96	49.80 (52.97)
20	55.10 (55.40)	53.91 (57.56)	26.17	61.41 (54.84)	62.12	56.00 (59.63)
25	59.80 (60.57)	58.63 (62.00)	32.03	67.11 (61.81)	67.94	61.06 (65.35)
30	63.47 (64.96)	62.18 (65.25)	37.46	70.53 (65.98)	71.52	65.44 (69.97)
35	67.54 (68.36)	65.33 (68.40)	42.63	73.03 (69.08)	73.93	69.80 (73.80)
40	69.57 (70.81)	67.47 (71.02)	46.68	75.02 (71.47)	75.31	73.20 (76.99)

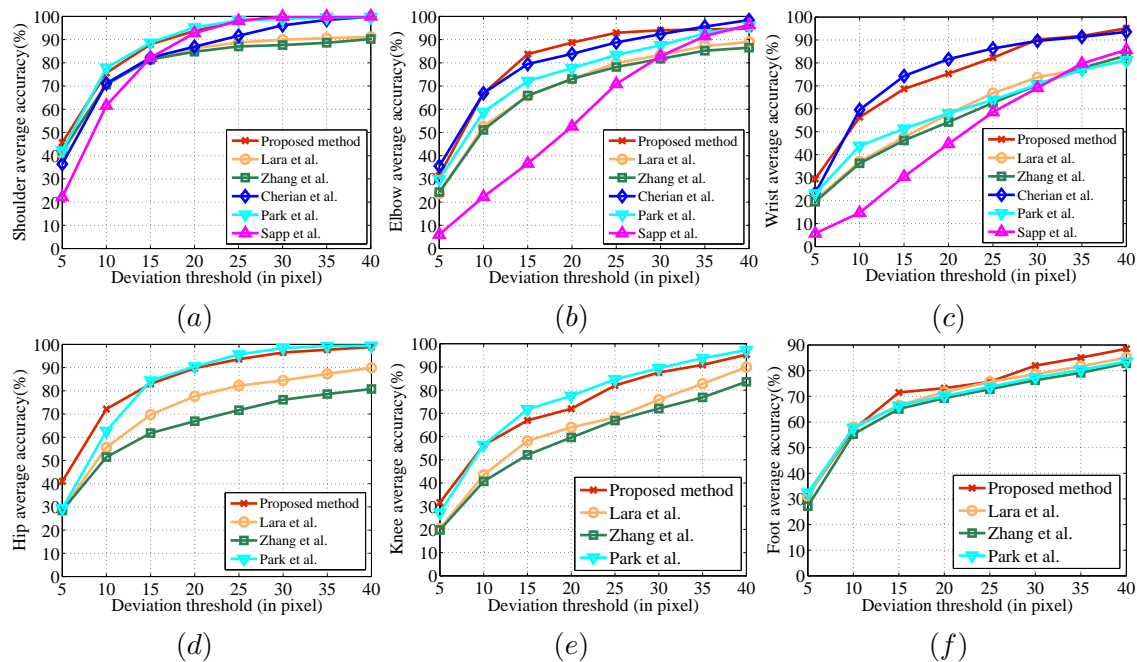


Fig. 18. Comparison results of different body parts with the state-of-the-art methods on Outdoor Pose dataset: (a) shoulder, (b) elbow, (c) wrist, (d) hip, (e) knee, and (f) foot.

shown in Table V. Ramakrishna et al. [35] have reported their result using *Percentage of Correct Parts* (PCP) [18] evaluation metric. So in Table VI we present PCP score of our method for comparison with [35], which reveals that on an average our method is superior.

To show the strength of the spatial constraints we run our experiment on four datasets (VideoPose2,

TABLE V
AVERAGE ACCURACY (IN %) OF POSE TRACKING COMPRISING SIX PARTS (SHOULDER, ELBOW, WRIST, HIP, KNEE, AND FOOT) TOGETHER USING DIFFERENT METHODS ON OUTDOOR POSE DATASET.

Dev. thrs. (in pixel)	Different methods					
	Lara [41]	Zhang [56]	Sapp [39]	Park [30]	Cherian [9]	Proposed
5	28.23 (27.46)	28.64 (26.89)	11.28	31.68 (30.68)	31.70	35.50 (35.05)
10	53.61 (52.98)	52.66 (50.90)	32.87	60.17 (59.54)	65.85	66.25 (64.04)
15	64.88 (64.82)	64.52 (62.09)	49.74	70.72 (72.44)	78.67	80.13 (76.97)
20	72.33 (71.71)	70.68 (67.97)	63.37	77.01 (78.19)	84.15	85.90 (82.10)
25	78.49 (76.93)	75.96 (73.21)	75.87	81.85 (83.25)	88.90	91.06 (87.41)
30	82.34 (80.99)	79.91 (77.37)	83.95	85.64 (87.02)	92.70	94.63 (91.66)
35	85.08 (84.50)	83.87 (81.04)	90.41	89.77 (90.44)	95.13	95.37 (93.29)
40	87.07 (87.69)	86.67 (84.54)	94.02	92.21 (92.81)	97.26	96.60 (95.41)

TABLE VI
COMPARISON WITH [35] USING PERCENTAGE OF CORRECT PARTS (PCP) ON OUTDOOR POSE DATASET.

Different body parts	Ramakrishna [35]	Proposed
upper arm	0.86	0.94
lower arm	0.52	0.81
upper leg	0.95	0.94
lower leg	0.96	0.92
Average	0.82	0.90

Poses in the Wild, Outdoor Pose and ICDPose) without spatial deformation (WOSD) constraints (or $\lambda_2 = 0$ in Eq. (4)). Table VII shows the average accuracy (%) of WOSD constraint and with spatial deformation (WSD) constraint for different values of Ω . We have done a computational complexity analysis and time comparison with the other methods in the next Subsection IV-D.

D. Computational complexity

In Subsection III-D we have mentioned that the order of time complexity of our proposed method is $O(nMN)$, where n is the number of body parts under consideration, M the plausible locations of each part and N is the number of clusters for each of these locations due to relative spatial displacement. On the other hand, the time complexity of pose estimation method given in [30] is $O(nMN^2)$ and that of Cherian et al. [9] is even higher. So the proposed method is at least N times faster than the state-of-the-art pose estimation methods presented in [30] and [9].

We have already compared the average time required by feature computation methods in Subsection IV-C (Table I). We have also compared the execution time of the proposed tracking method with

TABLE VII
COMPARATIVE RESULTS BETWEEN WITHOUT SPATIAL DEFORMATION (WOSD) AND WITH SPATIAL DEFORMATION (WSD)
CONSTRAINT ON DIFFERENT DATASETS (IN AVERAGE ACCURACY OF ALL THE PARTS)

Dev. thrs. (in pixel)	VideoPose2 [39]		Poses in the Wild [9]		Outdoor Pose [35]		ICDPose	
	WOSD	WSD	WOSD	WSD	WOSD	WSD	WOSD	WSD
5	41.08	41.22	22.20	23.50	30.87	35.05	33.20	33.53
10	58.60	61.13	41.94	44.02	61.60	64.04	43.36	43.98
15	65.90	69.84	54.60	59.58	74.45	76.97	51.80	52.97
20	77.20	78.21	62.43	68.21	80.81	82.10	58.73	59.64
25	77.47	82.03	66.51	72.55	86.16	87.41	64.70	65.36
30	83.17	84.74	70.80	75.42	90.41	91.66	68.73	69.97
35	86.94	88.04	73.81	77.67	92.78	93.29	71.90	73.81
40	87.82	89.90	76.68	79.59	94.69	95.41	75.25	76.99

TABLE VIII
AVERAGE TIME COMPARISON (IN SEC./FRAME) OF PROPOSED METHOD WITH THE STATE-OF-THE-ART INDIVIDUAL
TRACKING METHODS ON DIFFERENT DATASETS.

Datasets	Lara [41]	Zhang [56]	Proposed
VideoPose2 [39]	0.6293	0.0411	0.2268
Poses in the Wild [9]	0.6265	0.0518	0.2256
ICDPose [38]	1.1666	0.2375	0.4638
Outdoor Pose [35]	1.1720	0.2033	0.3904

that of the state-of-the-art individual object tracking methods [41], [56] in Table VIII, which shows that our method is slower than that of Zhang et al. [56]. However, the proposed method gives much higher accuracy compared to Zhang et al.’s method (see Tables II, III, VII, and V).

V. CONCLUSION

In this paper we have presented a human pose tracking method by introducing a novel body part descriptor. We have considered human pose as a graphical tree structure model and formulated the human pose tracking problem as a discrete optimization problem by combining the following terms: likeliness of appearance of a part within a frame, temporal displacement of the part from previous frame to the current frame, and spatial dependency of a part with its parent in the graph structure. The first and third terms take care of pose estimation in single frame or image, while the second term deals with object tracking in subsequent frames. More precisely the first term measures the degree of the presence of a body part at a location and the third term maintains the global structure of the human body. Thus the proposed method becomes robust by incorporating advantages of both approaches. We have proposed a greedy approach

to solve the optimization problem and consequently to track the human pose efficiently. Experimental results on benchmark datasets (VideoPose2, Poses in the Wild and Outdoor Pose) as well as on our newly developed full human body pose dataset, called ICDPose, show the efficacy of the proposed method.

REFERENCES

- [1] <http://people.csail.mit.edu/celiu/siftflow/>.
- [2] S.-H. Bae and K.-J. Yoon. Robust online multiobject tracking with data association and track management. *IEEE Trans. on Image Processing*, 23(7):2820–2833, 2014.
- [3] L. Ballan, M. Bertini, A. D. Bimbo, L. Seidenari, and G. Serra. Effective codebooks for human action representation and classification in unconstrained videos. *IEEE Trans. on Multimedia*, 14(4):1234–1245, 2012.
- [4] J. Bandouch, O. C. Jenkins, and M. Beetz. A self-training approach for visual tracking and recognition of complex human activity patterns. *IJCV*, 99(2):166–189, 2012.
- [5] M. Barnard, P. Koniusz, W. Wang, J. Kittler, S. M. Naqvi, and J. Chambers. Robust multi-speaker tracking via dictionary learning and identity modeling. *IEEE Trans. on Multimedia*, 16(3):864–880, 2014.
- [6] H. Bay, A. Ess, T. Tuytelaars, and L. V. Gool. Surf: Speeded up robust features. *CVIU*, 110(3):346–359, 2008.
- [7] T. A. Biresaw, A. Cavallaro, and C. S. Regazzoni. Correlation-based self-correcting tracking. *Neurocomputing*, 152(3):345–358, 2015.
- [8] Z. Cai, L. Wen, Z. Lei, N. Vasconcelos, and S. Z. Li. Robust deformable and occluded object tracking with dynamic graph. *IEEE Trans. on Image Processing*, 23(12):5497–5509, 2014.
- [9] A. Cherian, J. Mairal, K. Alahari, and C. Schmid. Mixing body-part sequences for human pose estimation. In *CVPR*, June 2014.
- [10] C.-T. Chu, J.-N. Hwang, H.-I. Pai, and K.-M. Lan. Tracking human under occlusion based on adaptive multiple kernels with projected gradients. *IEEE Trans. on Multimedia*, 15(7):1602–1615, 2013.
- [11] D. Comaniciu, V. Ramesh, and P. Meer. Real-time tracking of non-rigid objects using mean shift. In *CVPR*, 2000.
- [12] Y. Cong, B. Fan, J. Liu, J. Luo, and H. Yu. Speeded up low rank online metric learning for object tracking. *IEEE Trans. on CSVT*, 25(6):922–934, 2015.
- [13] F. C. Crow. Summed-area tables for texture mapping. In *Proceedings of the ACM SIGGRAPH*, 1984.
- [14] N. Dalal and B. Triggs. Histograms of oriented gradients for human detection. In *CVPR*, 2005.
- [15] M. Dantone, J. Gall, C. Leistner, and L. V. Gool. Body parts dependent joint regressors for human pose estimation in still images. *IEEE Trans. on PAMI*, 36(11):2131–2143, 2014.
- [16] J. Deutscher and I. Reid. Articulated body motion capture by stochastic search. *IJCV*, 61(2):185–205, 2005.
- [17] P. F. Felzenszwalb and D. P. Huttenlocher. Pictorial structures for object recognition. *IJCV*, 61(1):55–79, 2005.
- [18] V. Ferrari, M. Marín-Jiménez, and A. Zisserman. Progressive search space reduction for human pose estimation. In *CVPR*, 2008.
- [19] J.-M. Guo, Y.-F. Liu, C.-H. Chang, and H.-S. Nguyen. Improved hand tracking system. *IEEE Trans. on CSVT*, 22(5):693–701, 2012.
- [20] A. Heili, A. López-Méndez, and J.-M. Odobez. Exploiting long-term connectivity and visual motion in crf-based multi-person tracking. *IEEE Trans. on Image Processing*, 23(7):3040–3056, 2014.

- [21] R. Horaud, M. Niskanen, G. Dewaele, and E. Boyer. Human motion tracking by registering an articulated surface to 3-d points and normals. *IEEE Trans. on PAMI*, 31(11):158–163, 2008.
- [22] Y.-G. Jiang, Q. Dai, T. Mei, Y. Rui, and S.-F. Chang. Super fast event recognition in internet videos. *IEEE Trans. on Multimedia*, 17(8):1174–1186, 2015.
- [23] S. X. Ju, M. J. Black, and Y. Yacoob. Cardboard people: A parameterized model of articulated image motion. In *2nd Int. Conf. on Automatic Face- and Gesture-Recognition*, 1996.
- [24] M. Kiefel and P. V. Gehler. Human pose estimation with fields of parts. In *ECCV*, pages 331–346, 2014.
- [25] J. Kwon and K. M. Lee. Highly nonrigid object tracking via patch-based dynamic appearance modeling. *IEEE Trans. on PAMI*, 35(10):2427–2441, 2013.
- [26] S. Lazebnik, C. Schmid, and J. Ponce. Semi-local affine parts for object recognition. In *BMVC*, 2004.
- [27] A. M. Lehrmann, P. V. Gehler, and S. Nowozin. A non-parametric bayesian network prior of human pose. In *ICCV*, pages 1281–1288, 2013.
- [28] D. G. Lowe. Distinctive image features from scale-invariant keypoints. *IJCV*, 60(2):91–110, 2004.
- [29] E. Maggio and A. Cavallaro. *Video Tracking: Theory and Practice*. Wiley, 2011.
- [30] D. Park and D. Ramanan. N-best maximal decoders for part models. In *ICCV*, 2011.
- [31] H. S. Park and Y. Sheikh. 3d reconstruction of a smooth articulated trajectory from a monocular image sequence. In *ICCV*, 2011.
- [32] T. Pfister, K. Simonyan, J. Charles, and A. Zisserman. Deep convolutional neural networks for efficient pose estimation in gesture videos. In *ACCV*, 2014.
- [33] L.-M. Po and C. Cheung. A new center-biased orthogonal search algorithm for fast block motion estimation. In *TENCON*, 1996.
- [34] J. Puwein, L. Ballan, R. Ziegler, and M. Pollefeys. Foreground consistent human pose estimation using branch and bound. In *ECCV*, pages 315–330, 2014.
- [35] V. Ramakrishna, T. Kanade, and Y. Sheikh. Tracking human pose by tracking symmetric parts. In *CVPR*, pages 3728–3735, June 2013.
- [36] V. Ramakrishna, D. Munoz, M. Hebert, J. A. Bagnell, , and Y. Sheikh. Pose machines: Articulated pose estimation via inference machines. In *ECCV*, pages 33–47, 2014.
- [37] D. Ramanan, D. A. Forsyth, and A. Zisserman. Strike a pose: Tracking people by finding stylized poses. In *CVPR*, 2005.
- [38] Soumitra Samanta and Bhabatosh Chanda. http://www.isical.ac.in/~vlrg/sites/default/files/soumitra/site/ss_icdpose.html.
- [39] B. Sapp, D. Weiss, and B. Taskar. Parsing human motion with stretchable models. In *CVPR*, 2011.
- [40] C. Schmaltz, B. Rosenhahn, T. Brox, and J. Weickert. Region-based pose tracking with occlusions using 3d models. *MVA*, 23(3):557–577, 2012.
- [41] L. Sevilla-Lara and E. Learned-Miller. Distribution fields for tracking. In *CVPR*, 2012.
- [42] L. Sigal, M. Isard, H. Haussecker, and M. J. Black. Loose-limbed people: Estimating 3d human pose and motion using non-parametric belief propagation. *IJCV*, 98(1):15–48, 2012.
- [43] A. W. M. Smeulders, D. M. Chu, R. Cucchiara, S. Calderara, A. Dehghan, and M. Shah. Visual tracking: An experimental survey. *IEEE Trans. on PAMI*, 36(7):1442–1468, 2014.
- [44] J. Tao, Y.-P. Tan, and W. Lu. Robust color object tracking with application to people monitoring. *International Journal of Image and Graphics*, 7(2):227–254, 2007.
- [45] A. Toshev and C. Szegedy. Deeppose: Human pose estimation via deep neural networks. In *CVPR*, June 2014.

- [46] P. Viola and M. Jones. Rapid object detection using a boosted cascade of simple features. In *CVPR*, 2001.
- [47] S. Wang, H. Lu, F. Yang, and M.-H. Yang. Robust superpixel tracking. *IEEE Trans. on Image Processing*, 23(4):1639–1651, 2014.
- [48] Y. Wu, M. Pei, M. Yang, J. Yuan, and Y. Jia. Robust discriminative tracking via landmark-based label propagation. *IEEE Trans. on Image Processing*, 24(5):1510–1523, 2015.
- [49] L. Xie, A. Natsev, X. He, J. Kender, M. Hill, and J. R. Smith. Tracking large-scale video remix in real-world events. *IEEE Trans. on Multimedia*, 15(6):1244–1254, 2013.
- [50] T. Xu, P. Peng, X. Fang, C. Su, Y. Wang, Y. Tian, W. Zeng, and T. Huang. Single and multiple view detection, tracking and video analysis in crowded environments. In *AVSS*, pages 494–499, 2012.
- [51] Y. Yang and D. Ramanan. Articulated human detection with flexible mixtures of parts. *IEEE Trans. on PAMI*, 35(12):2878–2890, 2013.
- [52] B. Yao and F.-F. Li. Action recognition with exemplar-based 2.5d graph matching. In *ECCV*, 2012.
- [53] X. Yu, H. W. Leong, C. Xu, and Q. Tian. Trajectory-based ball detection and tracking in broadcast soccer video. *IEEE Trans. on Multimedia*, 8(6):1164–1178, 2006.
- [54] Y. Yuan, H. Yang, Y. Fang, and W. Lin. Visual object tracking by structure complexity coefficients. *IEEE Trans. on Multimedia*, 17(8):1125–1136, 2015.
- [55] C. Zhang and Y. Rui. Robust visual tracking via pixel classification and integration. In *ICPR*, pages 37–42, 2006.
- [56] K. Zhang, L. Zhang, Q. Liu, D. Zhang, and M.-H. Yang. Fast visual tracking via dense spatio-temporal context learning. In *ECCV*, 2014.
- [57] K. Zhang, L. Zhang, and M.-H. Yang. Fast compressive tracking. *IEEE Trans. on PAMI*, 36(10):2002–2015, 2014.
- [58] S. Zhang, X. Yu, Y. Sui, S. Zhao, and L. Zhang. Object tracking with multi-view support vector machines. *IEEE Trans. on Multimedia*, 17(3):265–278, 2015.
- [59] Z. Zhang, H. S. Seah, C. K. Quah, and J. Sun. Gpu-accelerated real-time tracking of full-body motion with multi-layer search. *IEEE Trans. on Multimedia*, 15(1):106–119, 2013.
- [60] W. Zhong, H. Lu, and M.-H. Yang. Robust object tracking via sparse collaborative appearance model. *IEEE Trans. on Image Processing*, 23(5):2356–2368, 2014.